

See discussions, stats, and author profiles for this publication at: <https://www.researchgate.net/publication/320366522>

# Functionalization of 2D macroporous silicon under the high-pressure oxidation

Article in *Applied Surface Science* · October 2017

DOI: 10.1016/j.apsusc.2017.10.029

CITATIONS

0

READS

50

9 authors, including:



[Liudmyla Karachevtseva](#)

National Academy of Sciences of Ukraine

77 PUBLICATIONS 245 CITATIONS

[SEE PROFILE](#)



[Vasyl Peter Kladko](#)

National Academy of Sciences of Ukraine

303 PUBLICATIONS 664 CITATIONS

[SEE PROFILE](#)



[Wang Bo](#)

TÜV Süd Group

21 PUBLICATIONS 67 CITATIONS

[SEE PROFILE](#)



[Olena Stronska](#)

V. Lashkaryov Institute of semiconductor phy...

21 PUBLICATIONS 58 CITATIONS

[SEE PROFILE](#)

Some of the authors of this publication are also working on these related projects:



Polymer-nanoparticle coatings on macroporous silicon matrix [View project](#)



Development of novel sensor materials and sensors based on micromachining and nano-technologies [View project](#)

All content following this page was uploaded by [Oleg Lytvynenko](#) on 08 November 2017.

The user has requested enhancement of the downloaded file.



## Full Length Article

## Functionalization of 2D macroporous silicon under the high-pressure oxidation



L. Karachevtseva<sup>a,b,\*</sup>, M. Kartel<sup>b</sup>, V. Kladko<sup>a</sup>, O. Gudymenko<sup>a</sup>, Wang Bo<sup>b</sup>, V. Bratus<sup>a</sup>, O. Lytvynenko<sup>a</sup>, V. Onyshchenko<sup>a</sup>, O. Stronska<sup>a</sup>

<sup>a</sup> V. Lashkaryov Institute of Semiconductor Physics NAS of Ukraine, 41 Nauky Pr., 03028 Kyiv, Ukraine

<sup>b</sup> Ningbo University of Technology, No.55-155 Cui Bai Road, Ningbo 315016, China

## ARTICLE INFO

## Article history:

Received 15 August 2017

Received in revised form

28 September 2017

Accepted 5 October 2017

Available online 9 October 2017

## Keywords:

Macroporous silicon

Orthorhombic SiO<sub>2</sub> phase

P<sub>b</sub> centers

## ABSTRACT

Addition functionalization after high-pressure oxidation of 2D macroporous silicon structures is evaluated. X-ray diffractometry indicates formation of orthorhombic SiO<sub>2</sub> phase on macroporous silicon at oxide thickness of 800–1200 nm due to cylindrical symmetry of macropores and high thermal expansion coefficient of SiO<sub>2</sub>. P<sub>b</sub> center concentration grows with the splitting energy of LO- and TO-phonons and SiO<sub>2</sub> thickness in oxidized macroporous silicon structures. This increase EPR signal amplitude and GHz radiation absorption and is promising for development of high-frequency devices and electronically controlled elements.

© 2017 Elsevier B.V. All rights reserved.

## 1. Introduction

During the last two decades macroporous silicon has found application and further development in nano- and microelectronics, optics and optoelectronics due to easy manufacturing, structural and physical properties and the possibility of integration in chips. Macroporous silicon is a promising material for development of 2D photonic structures with the required geometry and large efficient surface [1,2]. This allows to develop sensors based on measurements of optical, electrical, photovoltaic and photoluminescence characteristics of macroporous silicon. Thus, macroporous silicon-based optical biosensors were designed to detect low concentrations of DNA [3]. The capacitive humidity sensors [4], gas- and biosensors of CMOS-compatible manufacturing and solar cells with efficiency up to 13% [5] were produced.

Possibilities to enhance the properties of structured surfaces were demonstrated using 2D macroporous silicon with SiO<sub>2</sub> coatings [6]. The critical points in absorbance are related to photonic

modes excitation as an “absorption” process that includes intensity of the diffracted beam. The effect of surface oxide layer on the photonic band structure of a macroporous silicon photonic crystal was calculated in [7]. The bandgap in oxidized structure is shifted to the higher frequencies as compared to the non-oxidized case; this is useful for selectors and filters of electromagnetic modes. A model of the resonance electron scattering on impurity states in an electric field of “silicon-nanocoating” heterojunction on macroporous surface and realization of the Wannier–Stark effect on randomly distributed surface bonds were confirmed [8,9]. The contribution of the electron-phonon interaction to the broadening parameter  $\Gamma$  of the Wannier–Stark ladder levels was investigated in oxidized macroporous silicon structures with arbitrary macropore distribution [10]. The obtained value of the Wannier–Stark ladder parameter  $\Gamma$  is much less than the adjacent level energy evaluated from the giant oscillations of resonance electron scattering on the surface states. The growth of the concentration of bridge-like oxygen atoms in Si–O–Si (transverse optical phonons) after oxidation of macroporous silicon is due to reduction of the dangling bond passivation in the absence of hydrogen.

In this paper, functionalization of 2D macroporous silicon after high-pressure oxidation was investigated. High-resolution X-ray diffractometry and the splitting energy of longitudinal (LO) and transverse (TO) phonons in IR absorption spectra were measured to identify structural features of oxidized macroporous silicon and to compare results with GHz absorption and electron paramag-

\* Corresponding author at: V. Lashkaryov Institute of Semiconductor Physics NAS of Ukraine, 41 Nauky Pr., Kyiv, 03028, Ukraine.

E-mail addresses: [lakar@isp.kiev.ua](mailto:lakar@isp.kiev.ua) (L. Karachevtseva), [nikar@kartel.kiev.ua](mailto:nikar@kartel.kiev.ua) (M. Kartel), [kladko@isp.kiev.ua](mailto:kladko@isp.kiev.ua) (V. Kladko), [gudymenko@ukr.net](mailto:gudymenko@ukr.net) (O. Gudymenko), [bo305@hotmail.com](mailto:bo305@hotmail.com) (W. Bo), [v.bratus@isp.kiev.ua](mailto:v.bratus@isp.kiev.ua) (V. Bratus), [lytvole@gmail.com](mailto:lytvole@gmail.com) (O. Lytvynenko), [onyshchenkovf@isp.kiev.ua](mailto:onyshchenkovf@isp.kiev.ua) (V. Onyshchenko), [stronska@isp.kiev.ua](mailto:stronska@isp.kiev.ua) (O. Stronska).

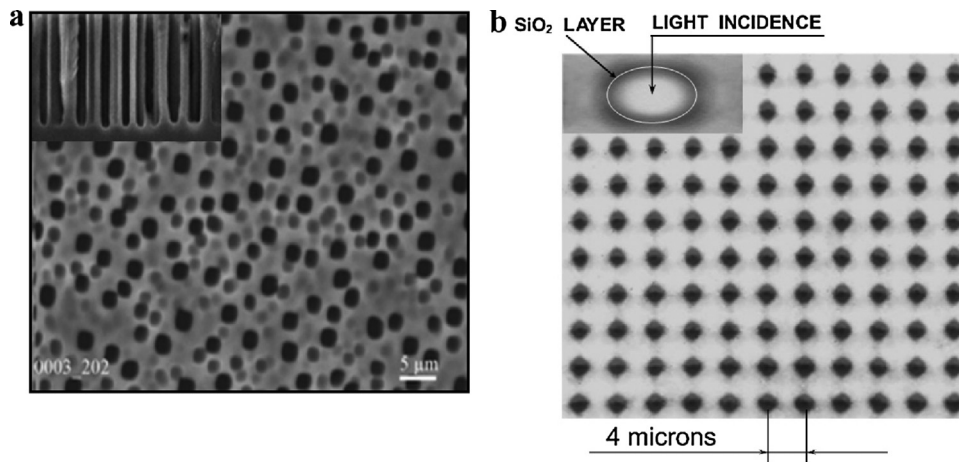


**Fig. 1.** a. The macroporous silicon structure with arbitrary macropore distribution. b. Oxidized macroporous silicon with square-lattice periodic structure; insertion: microphoto of the oxidized macropore with 800 nm SiO<sub>2</sub> thick (white circle is the initial macropore diameter) and scheme of the grazing incidence of IR radiation on the macropore surface (along the main axis of cylindrical macropores).

netic resonance (EPR) amplitude in oxidized macroporous silicon structures.

## 2. Procedure

The samples to be studied were made of *n*-type silicon wafers (thickness  $H = 520 \mu\text{m}$ ) characterized by the [100] orientation and with  $4.5 \Omega\text{-cm}$  resistivity. We used the standart technique of electrochemical etching at illumination of the back side of a silicon substrate [1,2]. Macropores of depth  $h_p = 60 \div 120 \mu\text{m}$  were formed due to the nonequilibrium holes generation and transfer to the *n*-Si electrochemically treated surface as a result of the optical band-to-band electron-hole generation. Macroporous silicon samples with arbitrary macropore distribution (Fig. 1a) were formed on nonhomogeneous of the substrate surface (the macropore diameter  $D_p = 2 \div 4 \mu\text{m}$  and the macropore concentration  $N_p = (1 \div 6)10^6 \text{cm}^{-2}$ ).

The square-lattice periodic macroporous structures were etched on Si substrates with relevant periodical pits of etching [1]. Period of structures  $a = 4 \mu\text{m}$ , diameter  $D_p = 2 \mu\text{m}$  and the macropore concentration  $N_p = 6.2,5 \times 10^6 \text{cm}^{-2}$ . The initial specimens are complex micropore-macropore silicon structures consisting of 150 nm micropore layers on macropore walls. Addition anisotropy etching for 30 s in 10% solution of KOH was used to remove the microporous layers from macropore walls.

SiO<sub>2</sub> coatings on macroporous silicon structures were formed in diffusion stove in the nitrogen atmosphere [6]. The  $5 \div 200 \text{ nm}$  thick oxide layers were formed on macroporous silicon samples in dry oxygen during  $15 \div 50 \text{ min}$  at a temperature of  $1050 \div 1200 \text{ }^\circ\text{C}$ . Silicon dioxide of  $800 \div 1200 \text{ nm}$  thick was formed at a temperature of  $1100 \text{ }^\circ\text{C}$  in wet oxygen using a steam generator with deionized water. The thickness of obtained SiO<sub>2</sub> layers was determined from the time of structure staying above the source of evaporation. The oxide thickness was measured with accuracy of 0.2 nm using ellipsometry.

High-resolution X-ray diffractometry was used to measure residual deformations in the oxidized macroporous silicon matrix. The measurements were carried out using a high-resolution diffractometer "PANalytical X'Pert PRO MRD" in the CuK $\alpha$  characteristic illumination [11]. The voltage on the X-ray tube was 45 kV and current was 40 mA. The symmetric curves of (004) reflection in X-ray refraction were measured. This made it possible to determine the silicon lattice parameter  $a$  along the normal to the structure surface (Fig. 1b) and the value of residual strain  $\Delta a$  in this direction. The

values of residual deformations were obtained relative to the lattice parameter of the original silicon plate. Grazing Incidence X-ray Diffraction (GIXRD) for film materials [12] was used to evaluate the SiO<sub>2</sub> phases in the samples. The reflex (004) of the silicon substrate is absent and does not interfere with the SiO<sub>2</sub> X-ray diffraction. The phase analysis was based on ICDD data.

The chemical states on the surface of macroporous silicon structures with coatings and the electric field at the "Si-SiO<sub>2</sub>" boundary were identified by IR absorption using a PerkinElmer Spectrum BXII IR Fourier spectrometer. The optical absorption spectra are recorded at normal incidence of IR radiation on the sample (along the main axis of cylindrical macropores – Fig. 1b, inset). The experiments are carried out at room temperature in the air. The error of spectral measurements is about  $2 \text{ cm}^{-1}$ . The sensitivity of light intensity is 0.5%.

The splitting energy of LO- and TO-phonons was measured in IR absorption spectra to identify structural features of oxidized macroporous silicon [10]. GHz absorption [13] and EPR signal intensity [14] were compared with the energy of LO- and TO-phonon splitting.

## 3. Experimental

### 3.1. High-resolution X-ray measurements

Parameters of macroporous silicon with SiO<sub>2</sub> nanocoatings measured by the high-resolution X-ray diffractometry are shown in Table 1.

The results of X-ray measurements of silicon lattice parameter  $a$ , the value of residual strain  $\Delta a$  and the omega scan half-width are shown in Table 2. The residual deformations are minimal for SiO<sub>2</sub> thickness of 20 nm. The maximal residual deformations were measured for a sample with SiO<sub>2</sub> thickness of 200 nm. The small residual deformations (Table 1) are determined from the presence of the vacancy-type defects [11]. The results of the omega scan half-width show that the samples 1–6 of macroporous silicon with SiO<sub>2</sub> thickness of  $5 \div 200 \text{ nm}$  have structural damages and coherent scattering from certain crystalline orientation in the macroporous silicon. The curves are measured parallel to the vector of the inverse lattice ( $2\theta$  omega scan) of these samples; they are symmetrical, without any deformation shoulders or tails. An increase in the half-width of the omega scans for the samples 5–6 indicates the appearance of structural defects of the reorientation type.

**Table 1**  
Parameters of oxidized macroporous silicon structures measured by high-resolution X-ray diffractometry.

Sample #	Dioxide thickness, $d_{\text{oxi}}$ , nm	Macropore depth, $h_p$ , $\mu\text{m}$	Macropore diameter, $D_p$ , $\mu\text{m}$	Macropore concentration, $N_p \times 10^6$ , $\text{cm}^{-2}$	Period of structures, $a$ , $\mu\text{m}$	Distance between oxidized macropores, $a - D_p - d_{\text{oxi}}$ , $\mu\text{m}$
1	0	71.4	3.5	3.1	5.7	2.2
2	4.8	73.3	3.2	1.5	8.2	5
3	11	72	3	3.2	5.6	2.6
4	19.5	75	3	3.6	5.3	2.3
5	54	80	4	2.3	6.6	2.6
6	203	72	4	2.3	6.6	2.4
7	800	68	3.5	1.6	7.9	3.6
8	1000	88	4	3.1	5.7	0.7
9	1200	120	4	1.6	7.9	2.7

**Table 2**  
Lattice parameter and residual strain for macroporous silicon with  $\text{SiO}_2$  nanocoatings.

Sample #	$\text{SiO}_2$ thickness, nm	Lattice parameter $a$ , $\text{\AA}$	$\Delta a/a$	Omega scan half-width
c-Si substrate	0	5.4307		9.3
1	0	5.4310	+ 0.0003	12.7
2	4.8	5.4308	+ 0.0001	16.3
3	11	5.4309	+ 0.0002	15.8
4	19.5	5.4307	0	21.9
5	54	5.4312	+ 0.0005	44.0
6	203	5.4319	+ 0.0012	43.5
7	800	5.4310	+ 0.0003	
8	1000	5.4310	+ 0.0003	
9	1200	5.4312	+ 0.0005	

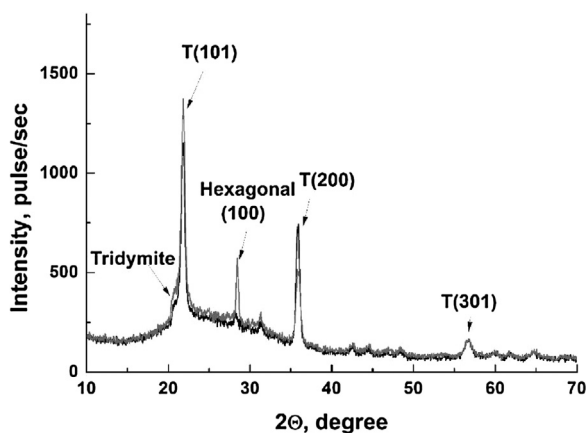


**Fig. 2.** X-ray diffractograms of the sample 7 (black curve 1) and sample 9 (grey curve 2) from Table 2. The letter T in front of the reflections points at the tetragonal phase.

Presence of  $\text{SiO}_2$  in the samples 1–6 of macroporous silicon is not fixed by GIXRD method [12] used to evaluate the  $\text{SiO}_2$  phases. But samples 7–9 (Tables 1 and 2) with a thick  $\text{SiO}_2$  layer have phases fixed with X-ray diffraction.

The X-ray diffractograms of the sample 7 (black curve) and the sample 9 (grey curve) from Table 2 are shown in Fig. 2. A small influx in the vicinity of 20.7 deg (Fig. 2) indicates formation of  $\beta$ -tridymite phase of  $\text{SiO}_2$  in samples 7 and 9 [15]. The hexagonal phase of  $\text{SiO}_2$  indicated by an additional peak at 29 deg is present in the sample 9 too (Fig. 2). Samples 7 and 9 have distance between oxidized macropores 3.6  $\mu\text{m}$  and 2.7  $\mu\text{m}$  (Table 1). Lower distance between oxidized macropores for sample 9 determines higher peaks in Fig. 2 indicated formation of  $\beta$ -tridymite phase of  $\text{SiO}_2$ , tetragonal and hexagonal phases of  $\text{SiO}_2$ .

The X-ray diffractograms of the sample 8 from Table 1 are measured for oxidized macroporous silicon (Fig. 3, curve 1) and for oxidized single-crystal silicon (Fig. 3, curve 2). Tetragonal  $\text{SiO}_2$  phase is formed in the oxidized single-crystal silicon. The data on oxidized macroporous silicon indicate formation of orthorhombic

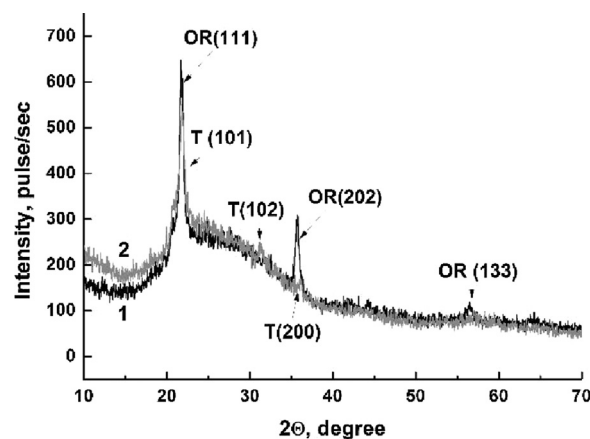


**Fig. 3.** X-ray diffractograms of oxidized macroporous silicon (curve 1) and oxidized single-crystal silicon (curve 2); T – tetragonal  $\text{SiO}_2$  phase, OR – orthorhombic  $\text{SiO}_2$  phase,  $\text{SiO}_2$  thickness is 1000 nm.

$\text{SiO}_2$  phase too ( $\beta$ -cristobalite, Fig. 4) [15]. A polymorphic transformation of  $\beta$ -tridymite to  $\beta$ -cristobalite (to orthorhombic  $\text{SiO}_2$  phase) occurs at the temperature of 1470  $^\circ\text{C}$  [16]. Silicon atoms form a diamond-type lattice in this highly symmetric modification to orthorhombic  $\text{SiO}_2$  phase (Fig. 4). Kinetics has a large effect on pressure induced phase transitions of  $\text{SiO}_2$ . The regime of pressure growth between macropores is realized under condition of different thermal expansion coefficients of silicon ( $2.6 \cdot 10^{-6} \text{ }^\circ\text{C}^{-1}$ ) and silicon dioxide ( $5.6 \cdot 10^{-7} \text{ }^\circ\text{C}^{-1}$ ). About 50% silicon dioxide grows in macropore volume and 50%  $\text{SiO}_2$  is formed within the macroporous silicon substrate ([17] and Fig. 1b, insertion). In our case, distance between oxidized macropores is minimal for sample 8 (0.7  $\mu\text{m}$ , Table 1). Samples 7 and 9 have 4–5 times higher distance between oxidized macropores. Thus, the higher pressure in silicon matrix between Si- $\text{SiO}_2$  boundaries allows formation in sample 8 the  $\beta$ -cristobalite with orthorhombic  $\text{SiO}_2$  phase in oxide at 1100  $^\circ\text{C}$  due to minimal distance between oxidized macropores, cylindrical

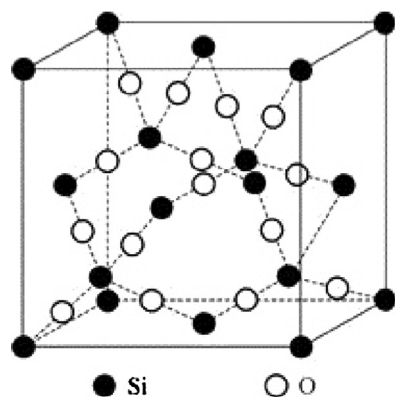


Fig. 4. Elementary cell of  $\beta$ -cristobalite [14].

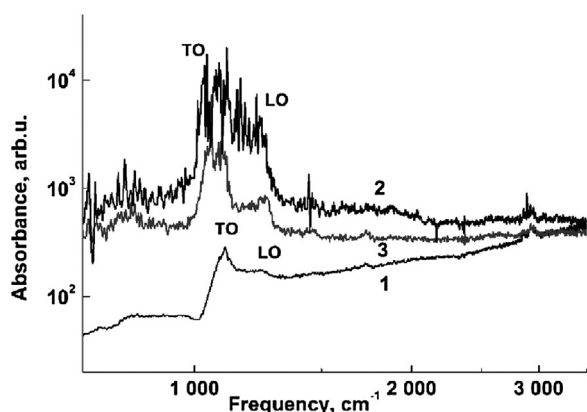


Fig. 5. IR absorption spectra of oxidized macroporous silicon structures with  $\text{SiO}_2$  thickness of: 1–7 nm, 2–15 nm, 3–30 nm.

symmetry of macropores and high thermal expansion coefficient of  $\text{SiO}_2$ .

### 3.2. The splitting energy of LO- and TO-phonons

Transverse (TO) and longitudinal (LO) optical phonons are Si–O vibrational modes in  $\text{SiO}_2$ , arising from the asymmetric Si–O stretching motions of  $\text{SiO}_4$  tetrahedra [18]. Fig. 5 shows IR absorption spectra of oxidized macroporous silicon structures with  $\text{SiO}_2$  thickness of 7 nm (curve 1), 15 nm (curve 2), 30 nm (curve 3) in the frequency area of TO- and LO-phonons. The splitting energy of LO- and TO- phonons in IR absorption spectra depends on the  $\text{SiO}_2$  thickness.

The splitting energy of LO- and TO-phonons determines stoichiometry on the border between Si and  $\text{SiO}_2$ , as well as residual strain and residual deformations [10]. The dependences of the splitting energy of LO- and TO- phonons (curve 1), the relative residual deformation  $\Delta a/a$  (curve 2) and the value of residual strain  $\Delta a$  (curve 3) vs the  $\text{SiO}_2$  thickness in oxidized macroporous silicon structures are shown in Fig. 6. The splitting energy of LO- and TO-phonons corresponds to growth of stoichiometry on the border between Si and  $\text{SiO}_2$  with  $\text{SiO}_2$  thickness increasing to 15–20 nm, to the maximal built-in charge in oxidized macroporous silicon structures and minimal residual strain [10] after its relaxation at oxide thickness of 20–50 nm. The minimum of the phonon splitting energy at  $d_{\text{OXI}} > 50$  nm corresponds to bend dependences of residual strain and the lattice parameter in macroporous silicon structures with a 50–200 nm  $\text{SiO}_2$  layer.

The maximal residual deformations at  $d_{\text{OXI}} = 200$  nm (Fig. 6, curves 2 and 3) correspond to phonon splitting energy bending (Fig. 6, curve 1). Perhaps this is due to structural  $\text{SiO}_2$  reorgani-

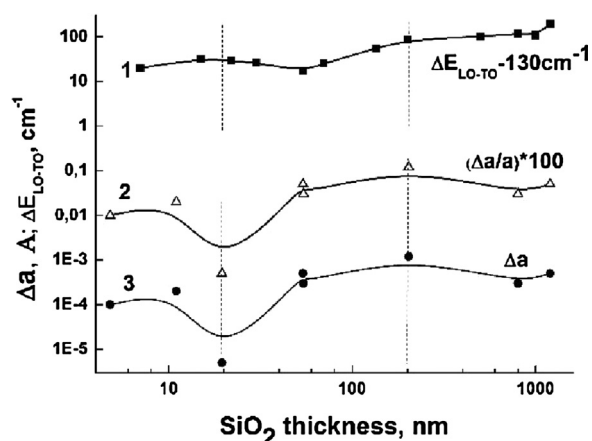


Fig. 6. Dependences of the splitting energy of LO- and TO-phonons (1), the relative residual deformation  $\Delta a/a$  (2) and the value of residual strain  $\Delta a$  (3) vs the  $\text{SiO}_2$  thickness in oxidized macroporous silicon structures.

zation. It is confirmed by the X-ray phase analysis: the presence of tridimite phase of  $\text{SiO}_2$  (Fig. 2) and  $\beta$ -cristobalite with orthorhombic phase of  $\text{SiO}_2$  (Fig. 3) formed under high pressure for thick  $\text{SiO}_2$  (800–1200 nm) [15]. In addition, slowing of the stress growth (Fig. 6) may be related to their relaxation due to formation of dislocations at  $\text{SiO}_2$  thickness over 200 nm [17].

### 3.3. Local states in oxidized macroporous silicon

IR absorption spectra in the frequency area of Si–H, C–H and OH local states of oxidized macroporous silicon structures are shown in Fig. 7a for  $\text{SiO}_2$  thickness of 15 nm (curve 1) and  $\text{SiO}_2$  thickness of 70 nm (curve 2). Fig. 7b shows the dependences of the energy splitting of LO- and TO- phonons (curve 1), the relative residual deformation  $\Delta a/a$  (curve 2) and IR absorption maxima of Si–H, C–H and OH local states (curves 3–5) on the  $\text{SiO}_2$  thickness in oxidized macroporous silicon structures. The minima of Si–H, C–H and OH bonds absorption correspond to maximal energy splitting of LO- and TO- phonons on the border between Si and  $\text{SiO}_2$  at  $\text{SiO}_2$  thickness of 15 nm under the condition of maximal stoichiometry. The maximum of OH bonds absorption (Fig. 7a, curve 2 and Fig. 7b, curve 3) correspond to maximal energy splitting of LO- and TO- phonons. The maximal residual deformations ( $\Delta a/a$ ) for 200 nm thick  $\text{SiO}_2$  (Fig. 7b, curve 2) determines the maximal concentration of Si–H and C–H bonds (Fig. 7b, curves 4 and 5). Thus, stoichiometry and residual deformations on the border between Si and  $\text{SiO}_2$  in oxidized macroporous silicon structures correlate with the hydrogen bonds concentration.

IR absorption spectra in the frequency area of  $P_{b0}$  centers with energy  $E_v + 0.85$  eV and  $P_{b1}$  centers with energy  $E_v + 0.80$  eV [19] are shown in Fig. 8a for  $\text{SiO}_2$  thickness of 15 nm (curve 1) and  $\text{SiO}_2$  thickness of 1000 nm (curve 2). Fig. 8b shows the dependences of the LO- and TO-phonons energy splitting (curve 1),  $P_{b0}$  center and  $P_{b1}$  center IR absorption maxima (curve 3) on the thickness of  $\text{SiO}_2$  in oxidized macroporous silicon structures.  $P_b$  center concentration increases with the splitting energy of LO- and TO-phonons and the thickness of  $\text{SiO}_2$  in oxidized macroporous silicon.

### 3.4. EPR signal intensity and GHz radiation absorption

Fig. 9 shows the dependences of the LO- and TO-phonons energy splitting (curve 1), the relative residual deformation  $\Delta a/a$  (curve 2),  $P_{b0}$  center IR absorption maxima (curve 3), EPR signal amplitude (curve 4) and GHz radiation absorption (curve 5) vs the thickness of  $\text{SiO}_2$  in oxidized macroporous silicon structures. The maximal

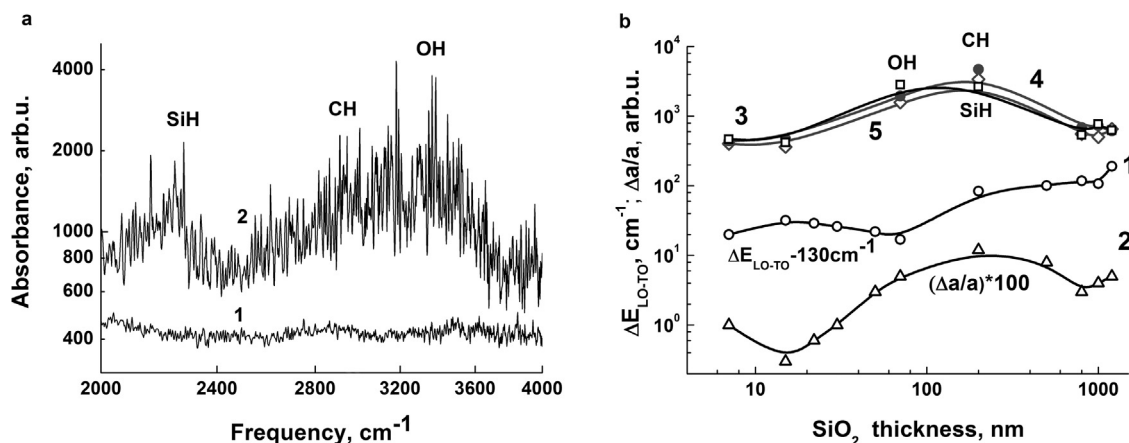


**Fig. 7.** a. IR absorption spectra in area of Si—H, C—H and OH local states of oxidized macroporous silicon structures with  $\text{SiO}_2$  thickness of: 1–15 nm, 2–70 nm. b. The LO- and TO- phonons energy splitting (1), the relative residual deformation  $\Delta a/a$  (2) and IR absorption maxima of Si—H, C—H and OH local states (3–5) vs the  $\text{SiO}_2$  thickness in oxidized macroporous silicon structures.

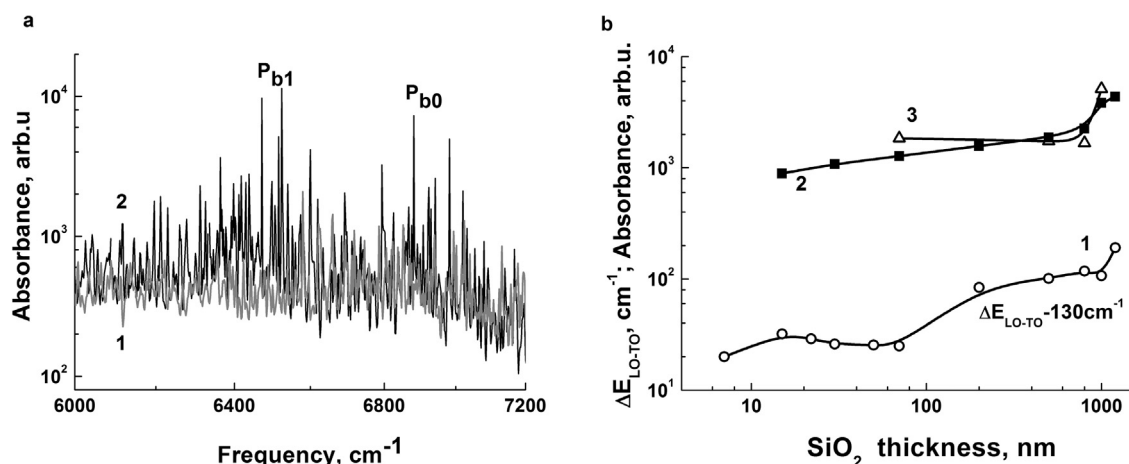


**Fig. 8.** a. IR absorption spectra in area of  $P_{b0}$  and  $P_{b1}$  local states of oxidized macroporous silicon structures with  $\text{SiO}_2$  thickness of: 1–15 nm, 2–1000 nm. b. Dependences of the LO- and TO- phonons energy splitting (1),  $P_{b0}$  (2) and  $P_{b1}$  (3) center IR absorption maxima on the  $\text{SiO}_2$  thickness in oxidized macroporous silicon structures.

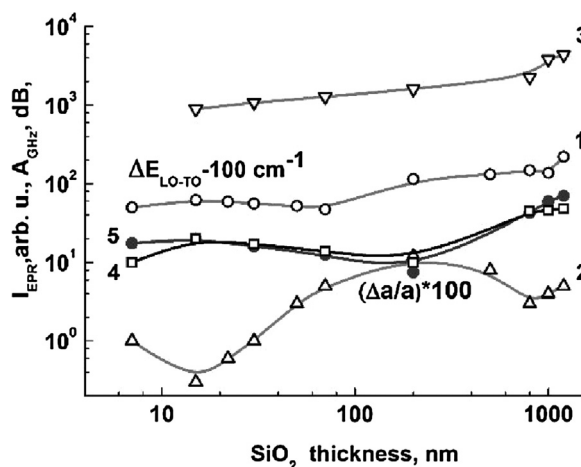


**Fig. 9.** The LO- and TO- phonons energy splitting (1), the relative residual deformation  $\Delta a/a$  (2),  $P_{b0}$  center IR absorption maxima (3), EPR signal intensity (4) and GHz radiation absorption (5) vs the  $\text{SiO}_2$  thickness in oxidized macroporous silicon structures.

residual deformations in  $\text{SiO}_2$  layer 200 nm thick essentially diminish GHz absorption and EPR signal. The EPR signal amplitude (curve 4) and GHz radiation absorption (curve 5) have minima at  $\text{SiO}_2$

thickness of 200 nm and increase at  $d_{\text{SiO}_2} > 200$  nm with growth of the LO- and TO- phonons energy splitting (curve 1), the relative residual deformation  $\Delta a/a$  (curve 2) and  $P_{b0}$  center IR absorption (curve 3). The dependences of EPR signal amplitude and GHz radiation absorption vs the  $\text{SiO}_2$  thickness (Fig. 8) are almost the same and have a common nature. Thus, structural  $\text{SiO}_2$  reorganization at  $d_{\text{SiO}_2} > 200$  nm changes paramagnetic  $P_b$  center concentration as a result of  $\beta$ -cristobalite with orthorhombic  $\text{SiO}_2$  phase formation under high pressure that determines the EPR signal amplitude.

In addition, GHz electromagnetic waves are scattering on the Si- $\text{SiO}_2$  border with absorption when the time of electron surface scattering is higher than GHz frequency. Earlier we estimated that the electron scattering lifetime  $\tau = \hbar/\Gamma$  increases to  $10^{-10}$  s in macroporous silicon structures with oxide thicknesses of 7–200 nm [10]. This is related to increase of the oscillation amplitude in the IR absorption spectra (Fig. 5). An abrupt increase of the oscillation amplitude in the electro-optical effects is determined by a decrease of the broadening parameter  $\Gamma$ . This parameter determines the electron scattering lifetime  $\tau = \hbar/\Gamma$ . The effect of broadening on the amplitude of oscillations in the IR absorption spectra of macroporous silicon was obtained from the convolution of the “nonbroadened” oscillation amplitude with the Lorentz distribution. High oscillation amplitudes (Fig. 8a, curve 2) and low values of  $\Gamma$  ( $0.01 \div 10 \text{ cm}^{-1}$ ) determine the electron scattering lifetime  $10^{-10}$ – $10^{-9}$  s for macroporous silicon structures with oxide

thicknesses of 800–1200 nm. That is more than the used GHz frequencies  $(2-4)10^{11}\text{s}^{-1}$ . In addition, oxidized macroporous silicon structures with low electron scattering time  $\tau = 10^{-11}-10^{-12}\text{ s}$  [20] do not absorb GHz radiation.

#### 4. Conclusions

New functionalizations of 2D macroporous silicon were confirmed for structures with thick  $\text{SiO}_2$  layers. High-resolution X-ray diffractometry and the splitting energy of LO- and TO-phonons in IR absorption spectra were investigated to identify structural features of oxidized macroporous silicon and to compare the results with EPR signal intensity and GHz radiation absorption.

Tetragonal  $\text{SiO}_2$  phase is formed in the oxidized single-crystal silicon. Data on oxidized macroporous silicon with thick  $\text{SiO}_2$  (800–1200 nm) indicate the formation of orthorhombic  $\text{SiO}_2$  phase ( $\beta$ -cristobalite). Higher pressure in the silicon matrix forms the orthorhombic  $\text{SiO}_2$  phase in oxide due to low distance between oxidized macropores, cylindrical symmetry of macropores and high thermal expansion coefficient of  $\text{SiO}_2$ .

The splitting energy of LO- and TO-phonons depends on the  $\text{SiO}_2$  thickness. The maximum built-in charge in oxidized macroporous silicon structures at  $\text{SiO}_2$  thickness of 15–20 nm is formed under the condition of maximal stoichiometry and minimal residual deformations on the Si- $\text{SiO}_2$  boundary. The maximum of residual deformations at  $\text{SiO}_2$  thickness of 200 nm corresponds to bend of the splitting energy dependence on the  $\text{SiO}_2$  thickness. The reduction of residual deformation at  $d_{\text{SiO}_2} > 200\text{ nm}$  accompanied by slowing of stress growth and formation of tridimite and orthorhombic phases of  $\text{SiO}_2$  under condition of high pressure in thick  $\text{SiO}_2$  (800–1200 nm). The stoichiometry and residual deformations on the Si- $\text{SiO}_2$  border in oxidized macroporous silicon structures correlate with hydrogen bond concentration.  $P_b$  center concentration increases with the phonon splitting energy and  $\text{SiO}_2$  thickness.

Addition functionalization of 2D macroporous silicon is a result of the high-pressure oxidation. The structural  $\text{SiO}_2$  reorganization to orthorhombic phase increases the concentration of paramagnetic  $P_b$  centers, EPR signal amplitude and GHz radiation absorption. Thus, variation of the  $\text{SiO}_2$  layers thickness in oxidized macroporous silicon permits to change high-frequency signals. This is promising for development of filters and electronically controlled antennas.

#### Acknowledgments

This work was supported by the Project #2016010010 of Scientific and Technical Cooperation between the National Academy of Sciences of Ukraine and the Ningbo University of Technology (China). We are thankful to Prof. S. Tarapov for measurements of GHz radiation absorption.

#### References

- [1] V. Lehman, The physics of macropore formation in low doped n-Type silicon, *J. Electrochem. Soc.* 140 (1993) 2836–2843, <http://dx.doi.org/10.1149/1.2220919>.

- [2] L.A. Karachevtseva, O.A. Litvinenko, E.A. Malovichko, Stabilization of electrochemical formation of macropores in n-Si, *Theor. Exp. Chem.* 34 (1998) 287–291, <http://dx.doi.org/10.1007/BF02523264>.
- [3] M. Archer, Macroporous silicon electrical sensor for DNA hybridization detection, *Biomed. Microdevices* 6 (2004) 203–211, <http://dx.doi.org/10.1023/B:BMMD.0000042049.85425.af>.
- [4] Y. Wang, A capacitive humidity sensor based on ordered macroporous silicon with thin film surface coating, *Sens. Actuators B* 149 (2010) 136–142, <http://dx.doi.org/10.1016/j.snb.2010.06.010>.
- [5] M. Ernst, R. Brendel, R. Ferré, N.-P. Harder, Thin macroporous silicon heterojunction solar cells, *Phys. Stat. Sol. RRL* 6 (2012) 187–189, <http://dx.doi.org/10.1002/pssr.201206113>.
- [6] A. Glushko, L. Karachevtseva, Photonic band structure of oxidized macroporous silicon, *Opto-Electron. Rev.* 14 (2006) 201–203, <http://dx.doi.org/10.2478/s11772-006-0026-9>.
- [7] L. Karachevtseva, Yu. Goltviansky, O. Sapelnikova, O. Lytvynenko, O. Stronska, Wang Bo, M. Kartel, Wannier–Stark electro-optical effect, quasi-guided and protonic modes in 2D macroporous silicon structures with  $\text{SiO}_2$  coatings, *Appl. Surf. Sci.* 388 (2016) 120–125, <http://dx.doi.org/10.1016/j.apsusc.2016.03.026>.
- [8] A.M. Berezhevskii, A.A. Ovchinnikov, Influence of impurities on the Wannier–Stark ladder in semiconductor in a strong electric field, *Phys. Stat. Sol. (b)* 110 (1982) 455–459, <http://dx.doi.org/10.1002/pssb.2221100210>.
- [9] L. Karachevtseva, S. Kuchmii, O. Lytvynenko, F. Sizov, O. Stronska, A. Stroyuk, Oscillations of light absorption in 2D macroporous silicon structures with surface nanostructures, *Appl. Surf. Sci.* 257 (2011) 3331–3335, <http://dx.doi.org/10.1016/j.apsusc.2010.11.016>.
- [10] L. Karachevtseva, Yu. Goltviansky, O. Kolesnyk, O. Lytvynenko, O. Stronska, Wannier–Stark effect and electron–phonon interaction in macroporous silicon structures with  $\text{SiO}_2$  nanostructures, *Opto-Electron. Rev.* 22 (2014) 201–206, <http://dx.doi.org/10.2478/s11772-014-0199-6>.
- [11] V.P. Kladko, A.F. Kolomys, M.V. Slobodian, V.V. Strelchuk, V.G. Raycheva, A.E. Belyaev, S.S. Bukalov, H. Hardtdegen, V.A. Sydoruk, N. Klein, S.A. Vitusevich, Internal strains and crystal structure of the layers in AlGaIn/GaN heterostructures grown on a sapphire substrate, *J. Appl. Phys.* 105 (063515) (2009) 1–9, <http://dx.doi.org/10.1063/1.3094022>.
- [12] M. Bouroushian, T. Kusanovic, Characterization of thin films by low incidence X-ray diffraction, *Cryst. Struct. Theory Appl.* 1 (2012) 35–39, <http://dx.doi.org/10.4236/csta.2012.13007>.
- [13] V. Bratus', I. Indutnyi, P. Shepeliavyyi, T. Torchynska, An EPR investigation of  $\text{SiO}_x$  films with columnar structure, *Physica B.* 453 (2014) 26–28, <http://dx.doi.org/10.1016/j.physb.2013.11.060>.
- [14] S. Chernovtsev, D. Belozorov, S. Tarapov, Magnetically controllable 1D magnetophotonic crystal in millimetre wavelength band, *J. Phys. D: Appl. Phys.* 40 (2007) 295–299, <http://dx.doi.org/10.1088/0022-3727/40/2/001>.
- [15] A.F. Wright, A.J. Leadbetter, The structures of the  $\beta$ -cristobalite phases of  $\text{SiO}_2$  and  $\text{AlPO}_4$ , *Philos. Mag.* 31 (1975) 1391–1401, <http://dx.doi.org/10.1080/00318087508228690>.
- [16] V.P. Prakapenka, Guoyin Shen, L.S. Dubrovinsky, M.L. Rivers, S.R. Sutton, High pressure induced phase transformation of  $\text{SiO}_2$  and  $\text{GeO}_2$ : difference and similarity, *J. Phys. Chem. Solids* 65 (2004) 1537–1545, <http://dx.doi.org/10.1016/j.jpcs.2003.12.019>.
- [17] E.V. Astrova, T.N. Borovinskaya, T.S. Perova, M.V. Zamoryanskaya, Quartz microtubes based on macroporous silicon, *Semiconductors* 38 (2004) 1084–1087, <http://dx.doi.org/10.1134/1.1797490>.
- [18] K.T. Queeney, M.K. Weldon, J.P. Chang, Y.J. Chabal, A.B. Gurevich, J. Sapjeta, R.L. Opila, Infrared spectroscopic analysis of the Si/ $\text{SiO}_2$  interface structure of thermally oxidized silicon, *J. Appl. Phys.* 87 (2000) 1322–1330, <http://dx.doi.org/10.1063/1.372017>.
- [19] G.J. Gerardi, E.H. Poindexter, P.J. Caplan, N.M. Johnson, Interface traps and Pb centers in oxidized (100) silicon wafers, *Appl. Phys. Lett.* 49 (1986) 348–351, <http://dx.doi.org/10.1063/1.97611>.
- [20] L. Karachevtseva, S. Kuchmii, O. Stroyuk, O. Lytvynenko, O. Sapelnikova, O. Stronska, Wang Bo, M. Kartel, Light-emitting structures of CdS nanocrystals in oxidized macroporous silicon, *Appl. Surf. Sci.* 388 (2016) 288–293, <http://dx.doi.org/10.1016/j.apsusc.2016.01.069> 0169–4332.